Fuel 312 (2022) 122939

Contents lists available at ScienceDirect

Fuel

journal homepage: www.elsevier.com/locate/fuel

Full Length Article

Vanadium and nickel distributions in selective-separated *n*-heptane asphaltenes of heavy crude oils

Martha L. Chacón-Patiño [a], Jenny Nelson [b], Estrella Rogel [c], Kyle Hench [c], Laura Poirier [c], Francisco Lopez-Linares [c], Cesar Ovalles [c,*]

[a] National High Magnetic Field Laboratory, Florida State University, Tallahassee, FL 32310, USA
[b] Agilent Technologies, Inc., 5301 Stevens Creek Blvd, Santa Clara, CA 95051, USA
[c] Chevron Technical Center, 100 Chevron Way, Richmond, CA 94801, USA

ARTICLE INFO

Keywords:
Vanadium and nickel distributions
Selective-separation
Asphaltenes
Heavy crude oils

ABSTRACT

Understanding vanadium and nickel distributions in asphaltene fractions have significant commercial importance throughout the petroleum value chain and the potential use of heavy feedstocks as a precursor of carbon-based materials, such as carbon fibers. This work extends our previous studies and aims to characterize volatile and non-volatile vanadium and nickel distributions by selective separation of n-heptane asphaltenes obtained from two Venezuelan heavy crude oils and the NIST Standard Reference Material (SRM) 8505. Asphaltenes were separated by extrography, i.e., adsorption on SiO_2 and subsequent extraction with acetone, heptol (n-heptane/toluene 1:1 vol), and a mixture of toluene, THF, and methanol (TTM). The results suggest that their solubility and aggregation strongly correlate to a higher hydrogen deficiency and increased heteroatom levels. The qualitative analysis of the spent silica gel, containing irreversibly-adsorbed asphaltenes, by Light-Induced Breakdown Spectroscopy, suggests that regardless of the solvent power used during the extraction, strong chemisorbed Ni and V species remain on the SiO_2, presumable associated with porphyrin molecules present on such feeds. High-Temperature Gas Chromatography coupled with Inductively Coupled Plasma Mass Spectrometry (HTGC-ICP-MS) showed that vanadium and nickel compounds have boiling points starting at 1050 °F. Quantification of the V-content below 1300 °F for the Venezuelan crude 1 indicated that the acetone fraction contains a large amount of distillable vanadium (~62 %wt.). Interestingly, whole/unfractionated asphaltenes revealed only 47% of distillable vanadium, which suggests that the extrography method can obtain asphaltene fractions with "*improved*" properties (weaker aggregation, increased solubility, and lower boiling points). The characterization by atmospheric pressure photoionization Fourier Transform ion cyclotron resonance mass spectrometry (APPI FT-ICR MS) and HTGC-ICP-MS revealed that the acetone asphaltene fractions have a higher relative abundance of vanadyl porphyrins (with and without sulfur) than heptol and TTM.

1. Introduction

1.1. Importance of studying metal distributions in asphaltenes

Understanding vanadium and nickel distributions in asphaltene fractions have significant commercial importance throughout the petroleum value chain.[1–5] In upstream, metal-containing petroporphyrins are involved in asphaltene aggregation processes leading to formation damage, solid deposition downhole and surface installations, and reduced oil production rates.[6–8] In midstream, Vanadium (V-) and Nickel (Ni-) containing asphaltenes are deposited in storage tanks, vessels, and lines, affecting petroleum transportation from the production facilities to the refining centers.[9,10] Meanwhile in downstream, the presence of vanadium- and nickel-containing deposits leads to lower efficiency and reactivity of hydroprocessing,[11–13] furnace and heat exchanger fouling,[14–17], and catalyst poison and deactivation.[18,19] The immediate consequences are significant reductions in the refineries' reliability and profitability.[11,20]

Furthermore, due to their relatively high concentration of polycyclic aromatic hydrocarbons, asphaltenes are promising precursors for producing specialty carbon materials.[21] For example, active carbon,[22,23] carbon fibers,[24–26] carbon nanosheets,[27], and carbon foam

* Corresponding author.
E-mail address: covalles@chevron.com (C. Ovalles).

https://doi.org/10.1016/j.fuel.2021.122939
Received 21 October 2021; Received in revised form 2 December 2021; Accepted 10 December 2021
Available online 21 December 2021

[28] have been synthesized from petroleum- and coal-derived asphaltenes. Thus, if the chemical industry were to use asphaltene fractions as feedstocks, understanding the metal distributions is crucial to increase conversion and selectivity to produce the specialty mentioned above carbon materials as well as to enhance their performance.

1.2. Separations coupled to molecular characterization by ultra-high-resolution mass spectrometry

To gain more characterization knowledge, selective separation of petroleum-derived asphaltene fractions has been carried out by combining absorption on active surfaces (e.g., SiO_2) with low mass loading ($\leq$1%) and subsequent solvent extraction and chromatography, i.e., extrography.[29,30] Chacón-Patiño *et al.* separated asphaltene samples from diverse geological origins (e.g., Athabasca bitumen, Wyoming deposit, South American heavy/medium, Gulf of Mexico, Arabian heavy) by adsorption on silica, followed by Soxhlet extraction with two types of solvents. [31–33] The solvents were chosen first to produce monomeric asphaltenes efficiently and then, separation based on polarity. The first solvent series consisted of acetone and acetonitrile and were used for the selective extraction of remnant occluded/coprecipitated maltenes, low-molecular-weight aromatics, and vanadyl porphyrins. The second series of solvents was a polarity gradient using *n*-heptane (Hep), toluene (Tol), tetrahydrofuran (THF), and methanol (MeOH) to separate asphaltenes based on solubility. The authors analyzed the samples via atmospheric pressure photoionization with positive-ion APPI FT-ICR MS. They concluded that acetone/acetonitrile fractions efficiently produce non-aggregated ions (*m/z* range from ~ 200–1000 where *m/z* represents the ratio of an ion's mass (m) in atomic mass units (amu) to its formal charge (z). Formal charge is usually + 1), with ~ 50–100-fold ion production efficiency. Conversely, the later extracted materials (e.g., Hep/Tol and Tol/THF/MeOH) revealed much lower ionization efficiency, or "monomer ion yield." Thus, their mass spectrometry analysis is hampered by the decreased ion production. [34,35] MS and Tandem-MS results showed that the early eluting fractions (i.e., acetone and acetonitrile) were enriched in highly aromatic/alkyl-depleted island structures, which is consistent with "classical" asphaltene chemistry. On the other hand, the latter fractions revealed abundant archipelago structural motifs as well as species with atypical asphaltene molecular compositions: low aromaticity (double bond equivalents < 12) and high heteroatom content (up to 5–7 atoms per molecule, e.g., O_3S_2 class).[31] However, it has been pointed out that MS-derived atomic ratios (H/C, S/C, N/C) and compositional ranges should be taken cautiously because APPI – high-resolution MS is not inherently quantitative. Indeed, recent reports that used extrography separation for asphaltenes, followed by gel permeation chromatography with quantitation by ICP-MS and online detection by high-field FT-ICR MS, suggest the access to only ~ 30% of the Vanadium and S-containing species. The authors concluded that ions in APPI are preferentially produced from later-eluting GPC fractions, which indicates that "aggregation" impedes comprehensive MS analysis.[36] Regardless of this limitation, FT-ICR MS has allowed for access to the ultra-complexity of asphaltenes, revealing that island and archipelago structures coexist, and the dominance of one structural motif is sample-dependent. [35] Thus, FT-ICR MS has shown the extreme diversity of asphaltene molecules for several samples derived from different crude oils, exposing the coexistence of alkyl-depleted PAHs with DBE values from 20 to 40 and low heteroatom content, alkyl-enriched aromatics with DBEs between 10 and 35, and moderate content of heteroatoms, and low DBE species with "ultrahigh" heteroatom contents (polyfunctional compounds, e.g., class O_4S_3). Tandem-MS has enabled the detection of island and archipelago motifs for ions with varying degrees of aromaticity (DBE 15–35) and heteroatom content.[37]

1.3. The Boduszynski continuum applied to vanadium and nickel-containing compounds

Boduszynski found that the plots of vanadium and nickel contents, as a function of the increasing atmospheric equivalent boiling point (AEBP), have bimodal distribution patterns, showing a little "hump" in the vacuum gas oil (VGO) boiling range.[38,39] As previously reported by other authors, these metals present in crude oils seem to concentrate in the asphaltene fraction.[2,40–44]. Some heavy VGO, depending on the origin, might exhibit increased amounts of vanadium, readily detected as vanadyl porphyrins or $N_4O_1V_1$ class by FT-ICR MS. [39] In our previous work, we reported qualitative characterization of volatile and non-volatile vanadium and nickel distributions in entrained pentane-extracted (C5) maltenes, in-between C5-C7 asphaltenes, and n-heptane asphaltenes separated by solvent-extraction from two Venezuelan heavy crude oils and the NIST Standard Reference Material (SRM) 8505 [33]. The results demonstrated that the boiling points of V-containing species in asphaltenes, accessed via High-Temperature Gas Chromatography with Inductive Coupled Plasma Mass Spectrometry (HTGC-ICP-MS), feature a bimodal/multimodal distribution. Furthermore, positive-ion APPI FT-ICR MS revealed that the compositional range of vanadyl and nickel porphyrins is multimodal in terms of aromaticity or double bond equivalents (DBE = rings plus double bonds). For instance, $N_4O_1V_1$ and $N_4O_2V_1$ (with an additional oxygen atom) classes exhibited abundant compounds with DBE values of $\leq$ 22. However, the "aromaticity" increased in 4–6 DBE values for vanadyl porphyrins containing one sulfur atom.[33] The authors hypothesized that this compositional feature could be the reason behind the bimodal/multimodal nature of the observed boiling point distributions. Ni-containing porphyrins showed two major homologous series, which pointed toward a bimodal chemical nature but less extension than the vanadium homologs.[33]

This work extends our previous studies from the analysis of entrained pentane-extracted (C5) maltenes, in-between C5-C7 asphaltenes, and n-heptane asphaltenes to a detailed separation and characterization of the latest fraction. Furthermore, it aims to characterize volatile and non-volatile vanadium and nickel distributions by selective extraction of n-heptane asphaltenes obtained from two Venezuelan heavy crude oils and the NIST Standard Reference Material (SRM) 8505. Asphaltenes were separated by extrography on SiO_2 and subsequent extraction with acetone, heptol (n-heptane/toluene 1:1 vol), and a mixture of toluene, THF, and methanol (TTM). As in our previous work, the characterization was carried out by elemental analyses, asphaltene solubility profile, SEC, HTGC-ICP-MS, and APPI FT-ICR MS. [33]

2. Material and methods

2.1. Materials and methods

All solvents used were high-performance liquid chromatography (HPLC)-grade unless otherwise noted. The Venezuelan heavy crude oil **1** has 7.7° API gravity, 7.2 wt% C7-asphaltenes and a viscosity of 7.8 Pa s at 60 °C. The Venezuelan heavy crude oil **2** has 9.5° API gravity, 12.4 wt % C7-asphaltenes and a viscosity of 18.86 Pa s at 40 °C. The NIST Standard Reference Material (SRM) 8505 has 12° API gravity, 9.5 wt% C7-asphaltenes and a viscosity of 1.88 Pa s at 50 °C. The HT SIMDIS SD-SS3E-05 standard (Separation Systems, INC), 2,3,7,8,12,13,17,18-octaethyl-21H,23H-porphyrin vanadium oxide (Sigma Aldrich; USA), 5,10,15,20-tetraphenyl-21H,23H-porphine vanadium (IV) oxide (Sigma Aldrich), 2,3,7,8,12,13,17,18- octaethyl-21H,23H– porphyrin nickel (Sigma Aldrich) were used for calibration purposes. Silica gel was dried overnight at 120 °C before adsorption.

Elemental analyses were carried out (CHN) for the petroleum/asphaltene samples using a Thermo Scientific™ FLASH 2000 CHNS/O (Thermo Fisher Scientific. USA). Metal analyses were performed adapting a previously reported procedure as described in our previous

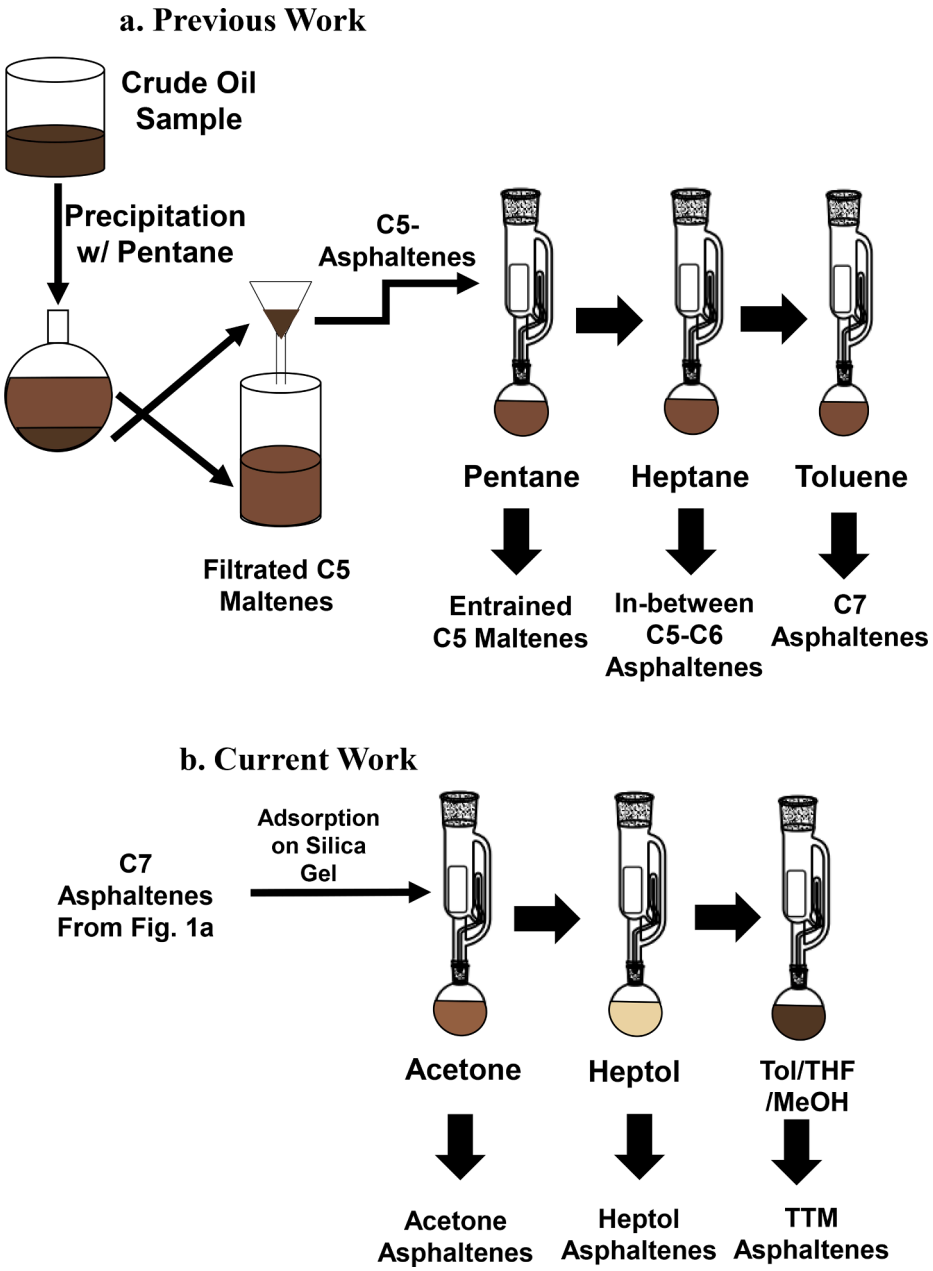

Fig. 1. Separation of C7-asphaltenes in our previous work [33] (Fig. 1a, i.e., solvent extraction with n-pentane, n-heptane, and toluene) and the current work (Fig. 1b, i.e., adsorption on silica gel, followed by solvent extraction with acetone, heptol (n-heptane/toluene = 1:1), and Tol/THF/methanol).

work.[33,45]

The spent SiO_2 with remnant/irreversibly adsorbed asphaltenes (after extrography separation) was analyzed using a J200 Tandem LIBS/LA instrument (Applied Spectra, Inc., Sacramento, CA) to assess the elemental composition. It is equipped with a 266 nm Nd: YAG laser (nanosecond), a six-channel CCD broadband spectrometer with a spectral window of 185 – 1050 nm, and a gas purged sample chamber. Full spectra were collected for each laser pulse; however, the main elements of interest were C 193.1 nm, H 656.3 nm, Ni 341.2 nm, Si 288.2 nm, V 409.26 nm, O 777.40 nm. The system is fully integrated and controlled using Applied Spectra's Axiom 2.0 operation software. High purity helium and argon gas (Airgas Inc., Concorde, CA) were used for all experiments to purge the sample chamber of any atmospheric gases. Experimental conditions are the following: argon carrier gas (0.5 mL/min), fluence (23 J/cm^2), spot size (75 um), gate delay (0.1 us), and repetition rate of 10 Hz, respectively. All the data (spectra and elemental maps) was analyzed using Applied Spectra's (Aurora) data analysis software (Aurora).

2.2. Asphaltene fractionation

Fig. 1 shows where our previous work finished [33], and the current one starts. First, the separations of C7-asphaltenes from the three heavy crude oils were carried in three steps. N-pentane was used to obtain the C5-asphaltenes, which, in turn, were exhaustively extracted with pentane to isolate the entrained C-5 Maltenes (Fig. 1a). Next, n-heptane was used to separate the In-between C5-C7 asphaltenes (n-pentane insoluble / n-heptane soluble, Fig. 1a) and toluene to solubilize the C7-asphaltenes (n-pentane/n-heptane insoluble, toluene soluble, Fig. 1a). [33] The last fraction, i.e., C7-asphaltenes, was adsorbed on silica gel ($\leq$10 mg of asphaltenes per gram of SiO_2) and Soxhlet extracted with acetone (Fig. 1b), n-heptane/Toluene (1:1, heptol, Fig. 1b), and toluene/THF/methanol (TTM, Fig. 1b) mixture.[31,46,47]

In a typical separation, 800 mg of asphaltenes were dissolved in

Table 1
Yields (wt%, for the extrography separation) and mass balances obtained for the selective- separation of C7- asphaltenes using adsorption on silica gel, followed by elution with acetone, heptol, and toluene/tetrahydrofuran/methanol for the Venezuelan Crude Oil 1. The results for the Venezuelan Crude 2 and NIST SRM 8505 are reported in Tables 1S and 2S of the Supplementary Material, respectively.

	C7- Asphaltenes[a]	Acetone Asphaltenes[b]	Heptol Asphaltenes[c]	TTM Asphaltenes[d]	Mass Balance[e]
wt% Yields	–	20.0	38.9	35.5	94.4%
C (wt%)[f]	75.23	72.35	82.98	79.9	99.8%
H (wt%)[g]	6.81	7.26	8.14	7.00	104.3%
N (wt%)[h]	1.50	1.51	1.52	1.55	96.2%
H/C[i]	1.09	1.20	1.18	1.05	98.7%
Ni (mg kg^{-1})[j]	407	250	432	417	89.9%
V (mg kg^{-1})[k]	1850	1930	1880	1760	94.2%
S (wt%)[l]	4.43	3.54	4.34	5.03	94.4%

[a] As shown in Fig. 1, n-heptane (C7) asphaltene fraction was preparatively separated using n-pentane (C5/crude ratio of 10:1 at 25 °C for 6 h), followed by Soxhlet extraction using n-heptane and toluene.
[b] C7-asphaltenes were adsorbed on a silica gel column and eluted using acetone, [c]Eluted using heptol (n-heptane / toluene 1;1 vol)
[d] Eluted using toluene/tetrahydrofuran/methanol (TTM)
[e] Mass balances with respect to the C7-asphaltenes.
[f] Weight percentage of carbon by elemental analysis
[g] Weight percentage of hydrogen by elemental analysis
[h] Weight percentage of nitrogen by elemental analysis
[i] Hydrogen-to-carbon molar ratio
[j] Vanadium content as determined by ICP-OES
[k] Nickel content as determined by ICP-OES
[l] Weight percentage of sulfur by elemental analysis.

dichloromethane (200 mg/mL) and mixed with 160 g of SiO_2 (100–200 mesh, type 60 Å, Fisher Scientific). The mixture was entirely dried under N_2 (48 h, protected from light). The dried asphaltenes/SiO_2 were progressively extracted with acetone, heptol (1:1), and TTM (5:5:1) using a Soxhlet apparatus; each extraction lasted 24 h and was carried out under nitrogen atmosphere in the dark. After each extraction step, the mixture SiO_2/remnant asphaltenes was entirely dried under N_2.[31]

The unconventional solvent series facilitates the initial extraction of highly aromatic / *peri*-condensed structures with a high production efficiency of non-aggregated asphaltene ions in atmospheric pressure photoionization (APPI), which leaves behind the compounds challenging to ionize. Acetone is a polar solvent, but its predominant intermolar interactions are dipole–dipole, which promotes the extraction of alkyl-deficient PAHs, remnant occluded/entrained maltenes, and vanadyl porphyrins. The second solvent mixture, heptol, assists the isolation of alkyl-aromatic compounds. Finally, Tol/THF/MeOH promotes the extraction of asphaltene molecules that interact with the SiO_2 silanol groups via hydrogen bonding. This fraction contains abundant asphaltene species enriched with polarizable functionalities, which have revealed a poor ionization in APPI. All the collected fractions were dried (N_2) and stored in the dark for subsequent characterization.[31]

The yields (wt.%) and mass balances obtained for the selective-separation of C7- asphaltenes of the Venezuelan crude oil **1** are shown in Table 1. The results for the Venezuelan crude **2** and NIST SRM 8505 are reported in Tables 1S and 2S of the Supplementary Material, respectively.

2.3. Asphaltene analyses

The HPLC system consisted of HP Series 1100/Agilent Series 1200 instruments coupled to an Alltech Evaporative Light Scattering Detector (ELSD) 2000. The asphaltene solubility profiles were carried out at room temperature using n-heptane, then 10% methanol/90% dichloromethane (v/v), and finally 100% methanol and quantified using an evaporative light scanning detector (ELSD), as described elsewhere.[48] SEC was carried out using a 30 cm × 7.5 mm PL gel "mixed E" column. Sample solutions of 1000 mg kg^{-1} were prepared in CH_2Cl_2, and the elution was carried out with 90/10 CH_2Cl_2 /CH_3OH at a flow rate of 1.0 mL/min and a temperature of 25 °C.

2.4. GC-ICP-MS characterization

The V and Ni distribution along the boiling point was performed following the procedure previously reported.[49,50] Briefly, GC was interfaced to an Agilent 7700x ICP-MS (Agilent Technologies, Tokyo, Japan) through a commercially available heated GC-ICP-MS interface (Agilent Technologies, Santa Clara, CA, USA). Heated argon as a makeup gas was required to assist the flow of species through the heated transfer line (Ar gas is preheated by passing through a stainless-steel coil mounted in the GC oven). As reported elsewhere, a high temperature simulated distillation column, DB-HT-SIMDIS, 5 m, 0.530 mm id., 0.15 μm (Agilent Technologies Inc) was used.[49,50]

2.5. FT-ICR MS characterization

Asphaltenes were dissolved in toluene at a 50 μg/mL concentration and directly infused into an atmospheric pressure photoionization source (Thermo-Fisher Ion Max APPI source, San Jose, CA, U.S.A.) as reported previously.[49] Positive ions were analyzed with a custom-built 9.4 T Fourier transform ion cyclotron resonance mass spectrometer, equipped with a dynamically harmonized ICR cell. Broadband mass spectra, resulting from the coaddition of at least 100 scans, were internally calibrated with at least five extended homologous series covering the entire *m/z* range (>100 peaks). Peaks with a relative abundance above 6σ baseline root-mean-square (RMS) noise were exported for molecular formula assignment. PREDATOR and PetroOrg custom software-assisted data processing and visualization.[33]

2.6. Elemental analysis and chemical mapping of the spent SiO_2 by LIBS

The spentSiO_2 with remnant asphaltenes, after toluene/THF/methanol extraction of n-heptane asphaltenes from NIST SRM 8505 and Venezuelan Crude oil 2, were selected to investigate the elemental composition of "irreversibly" adsorbed. For that purpose, approx. 500 mg of each neat sample was pelletized (Spex model 3630) in a 13 mm SS Die, pressed with 10 tones, hold time of 3 min, and residual time of 1 min.

The resultant pellets were analyzed using J200 tandem instrument with the condition described in Section 2.1, and a 2D map was obtained using 36 parallel lines with 500 shots/lines covering a total area of 100 mm^2. Each data point in the elemental intensity maps is the integral of

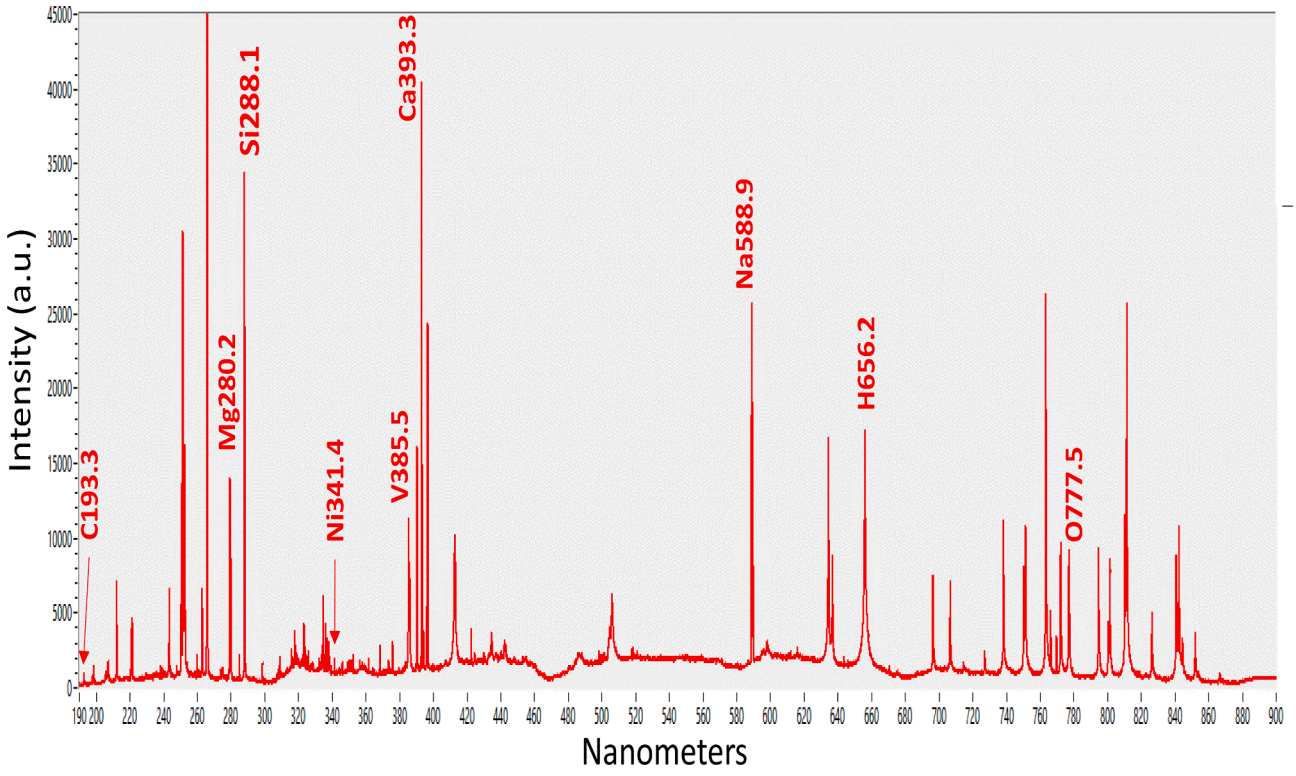

Fig. 2. Typical LIBS spectra (first shot). Main elements are included as a reference.

Table 2
Intensity ratio for the target elements on the spent silica.

Intensity ratio	NIST-8505	Venezuelan crude oil 2
C/Si	0.01	0.01
Ni/Si	0.05	0.08
V/Si	0.05	0.07
Ni/V	1.11	1.12

an elemental peak from the spectrum. Fig. 2 shows a typical LIBS spectrum (displaying 187– 940 nm for visual purposes) for the main elements presented on the SiO_2 used for NIST SRM 8505. The 2D maps are qualitative. The quantification of the signal intensity was out of the scope of this article.

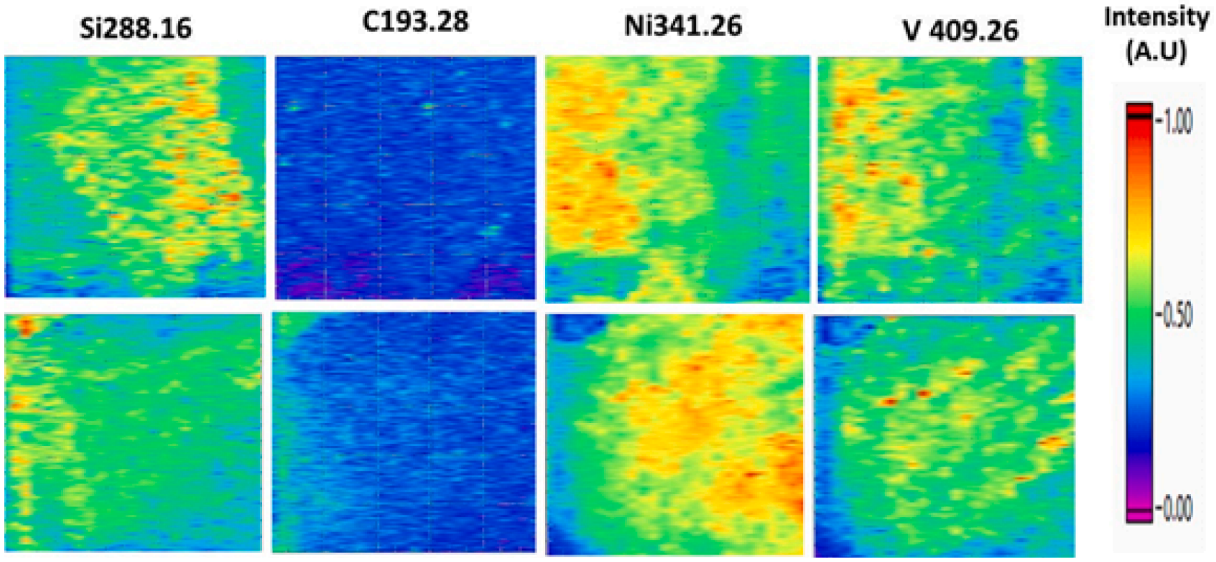

Fig. 3. Intensity maps of Si 288.16 nm, C 193.28 nm, Ni 341.26 nm, V 409.26 nm for NIST SRM 8505 (upper row) and Venezuela crude oil 2 (lower row). Since the plasma emission intensity differs for each element, the data sets were normalized by max intensity per element to facilitate visual comparison of these different components.

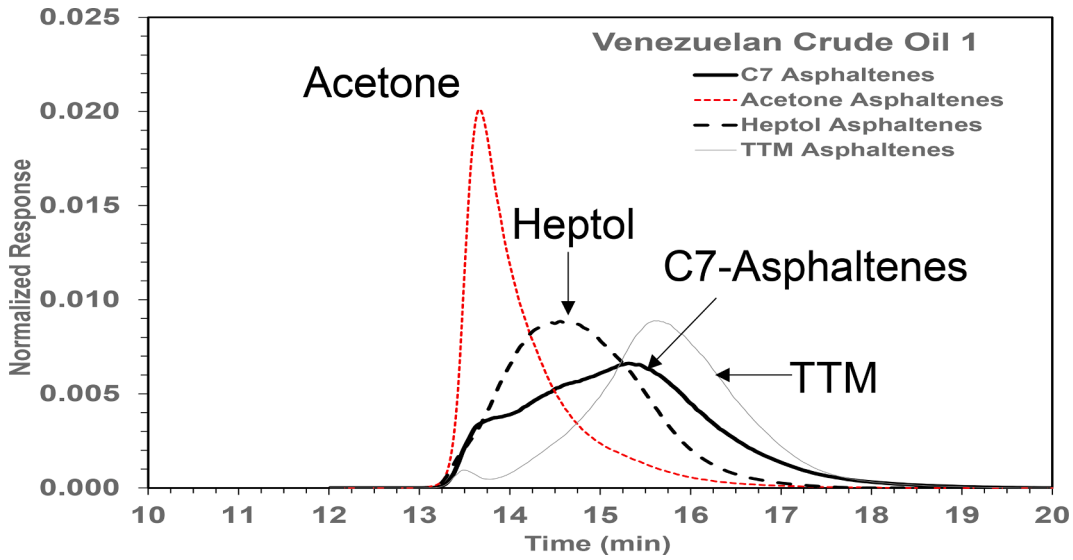

Fig. 4. Asphaltene solubility profile of the n-heptane (C7), acetone, heptol, and toluene/THF/Methanol extracted asphaltenes for Venezuelan crude oil 1. The results for the Venezuelan Crude 2 and NIST SRM 8505 are reported in Fig. 1S and Fig. 2S of the Supplementary Material.

3. Results and discussion

3.1. Mass balances and elemental analysis

Table 1 shows the percentages of yields (wt.%), mass balances, and elemental analysis for the separation of C7 asphaltenes by adsorption on silica gel, followed by Soxhlet extraction with acetone, heptol, and TTM for Venezuelan crude oil 1. The corresponding data for the Venezuelan crude 2 and NIST SRM 8505 are reported in Tables 1S and 2S of the Supplementary Material. In general, the heptol and TTM asphaltenes have the highest yields (30–40 wt%) than those found for the acetone-extracted fractions (18–23 wt%). As seen in Tables 1 and 2S, the mass balances with respect to the C7 asphaltenes for the Venezuelan crude 1 and NIST SRM 8505 are in the 89–104% range, respectively, indicating the validity of the data.[51]

For the Venezuelan crude oil 2, the material balances were significantly lower (79–93 %) than those obtained in the previous two cases. Thermogravimetric analysis (TGA) in air and temperatures up to 595 °C of the silica after solvent extraction showed the loss of ~ 6.2 wt%, indicating the presence of organic material deposited on the SiO_2. Elemental analysis by ICP-OES registered 0.5 mg kg^{-1} of nickel and 5.4 mg kg^{-1} of vanadium on the SiO_2 recovered. Thus, the lower mass balances obtained for the Venezuelan Crude 2 solvent separation were attributed to the irreversible adsorption of organic compounds on the silica gel.

At this point, we decided to obtain additional information related to the composition of residual organic material still present on the SiO_2 after extraction with all solvents. We propose using Laser-Induced Breakdown Spectroscopy (LIBS) to access the metals and non-metals contents and the H/C ratio. [52–56] LIBS is well-established to determine elemental analysis, requires minimal sample preparation, and can theoretically provide concentrations of every element on the periodic table of a given sample. [54,57] This analytical technique uses a pulsed, high-energy laser beam focused on the sample to produce a plasma. Characteristic spectral signatures of elements present in the sample are collected and analyzed to conclude the identity/abundance of the elements of interest. LIBS can perform a sample's surface (2D spatial) and depth analysis. [58,59]

In this sense, we decided to use LIBS to analyze each pellet to obtain elemental information. For such purpose, the resulting sample was used without further polishing or making the surface more homogenous. Thirty-six parallel lines with 500 shots/line, covering a total area of 100 mm^2, were used to gather the necessary data to build the 2D map. Each laser pulse that ablates the sample over the area has a unique spectrum corresponding to each location. These spectra can be used to reconstruct spatially selective chemical maps of these samples. Fig. 3 shows typical LIBS, qualitative chemical map for the main element selected on the SiO_2, used for the extrography separation of the NIST SRM 8505.

Each spectrum results from accumulating 500 laser pulses per line for an improved signal-to-background ratio. The atomic line for a given element (e.g., Si 288.169 nm) is integrated and reconstructed into a 2-D image using the x-y coordinates from the laser ablation method. This way, elemental maps for Si, C, Ni, Na, Mg, V, O, and H were detected in the extrography-spent silica gel. For this work, we focus on C, Si, Ni & V for the chemical mapping, as these are the main elements representing the solid matrix and the petroleum feedstock.

An initial assessment of the information gathered by mapping indicates element distributions on the silica surface. In both cases, Ni and V are adsorbed on the silica surface, regardless of the asphaltene source. Meanwhile, it is observed that C is homogeneously distributed on the surface compared to the metals. Interestingly, LIBS data suggest that the adsorption of Ni and V has the same preference for the Si sites; in other words, it is found the Ni & V adsorption occurs at the same area, as it is clearly noticed for NIST 8505 (Fig. 3, upper row). The presence of acidic sites associated with the silicon (Si-OH) could probably be the reason for the preferential deposition of the Ni- and V-containing compounds. For the Venezuelan crude oil 2, it is observed the same pattern with less definition (lower row). The element intensity was used to assess the element ratio on the surface. The data for both samples are presented in Table 2.

The intensity ratio was calculated using the intensity of the element from each spectrum associated with the map. No attempt to determine the sensitivity of the component and concentration was made. The sum of the intensity was calculated, and the ratio was determined accordingly. The data presented in Table 2 indicates that regardless of the feedstock, the carbon intensity on the SiO_2 surface is almost the same after using all solvents. Furthermore, in terms of the elements, the amount of Ni & V present on the SiO_2 surface for NIST 8505 is the same. In contrast, for the Venezuelan crude 2, Ni is slightly higher than V. It is also noticed that more metal remained on the surface when Venezuelan crude oil was used. Finally, the Ni/V ratio at the surface is almost the same for both samples.

The 2D qualitative chemical map data (Fig. 3) confirm the previous assumption: during the separation, regardless of the eluent strength of

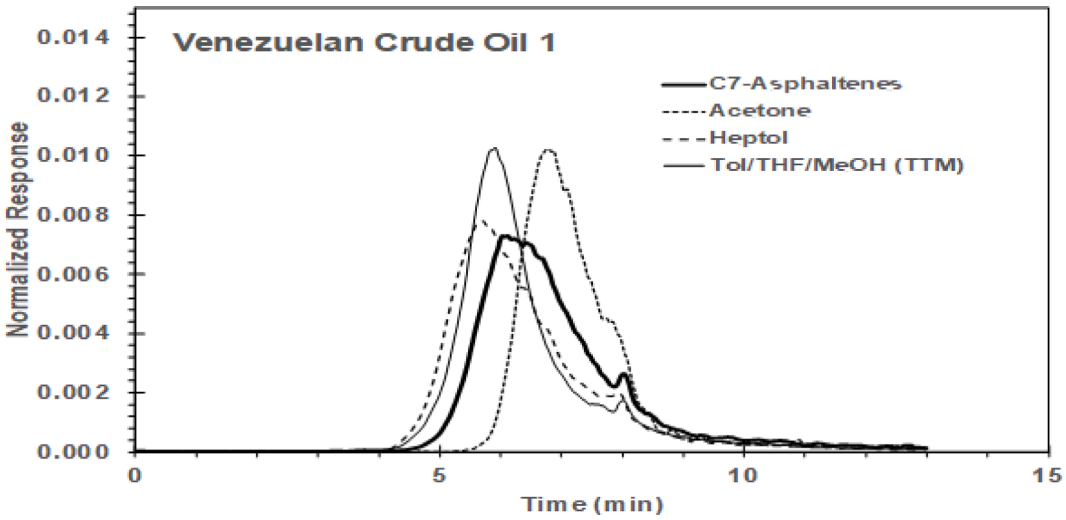

Fig. 5. Size exclusion chromatography of the n-heptane (C7), acetone, heptol, and Toluene/THF/Methanol extracted asphaltenes for Venezuelan crude oil 1. The results for the Venezuelan Crude 2 and NIST SRM 8505 are reported in Fig. 3S and Fig. 4S of the Supplementary Material.

the extracting solvent, some strong chemisorbed species remain on the SiO_2. Ni and V are dominant elements besides Si, suggesting these could be associated with porphyrin molecules present in the asphaltene fraction.

To detail the elemental composition of these new fractions, Table 1 shows that for Venezuelan Crude 1, the hydrogen-to-carbon molar ratio decreases, and the nitrogen and sulfur contents increase from acetone to heptol TTM extracted asphaltenes. As reported in the previous publication[33], the results indicate an increase in hydrogen deficiency and the content of heteroatoms and metals as the solvent changes from acetone to heptol and toluene-tetrahydrofuran-methanol. Similar results were obtained during the preparative separation of Mexican vacuum residue asphaltenes and a thermally cracked residue.[60]

Except for the nitrogen content (Table 2S), the asphaltenes separated from NIST SRM 8505 followed a similar trend as those for the Venezuelan Crude **1**, i.e., the H/C molar ratio decreased, and the N- and S-

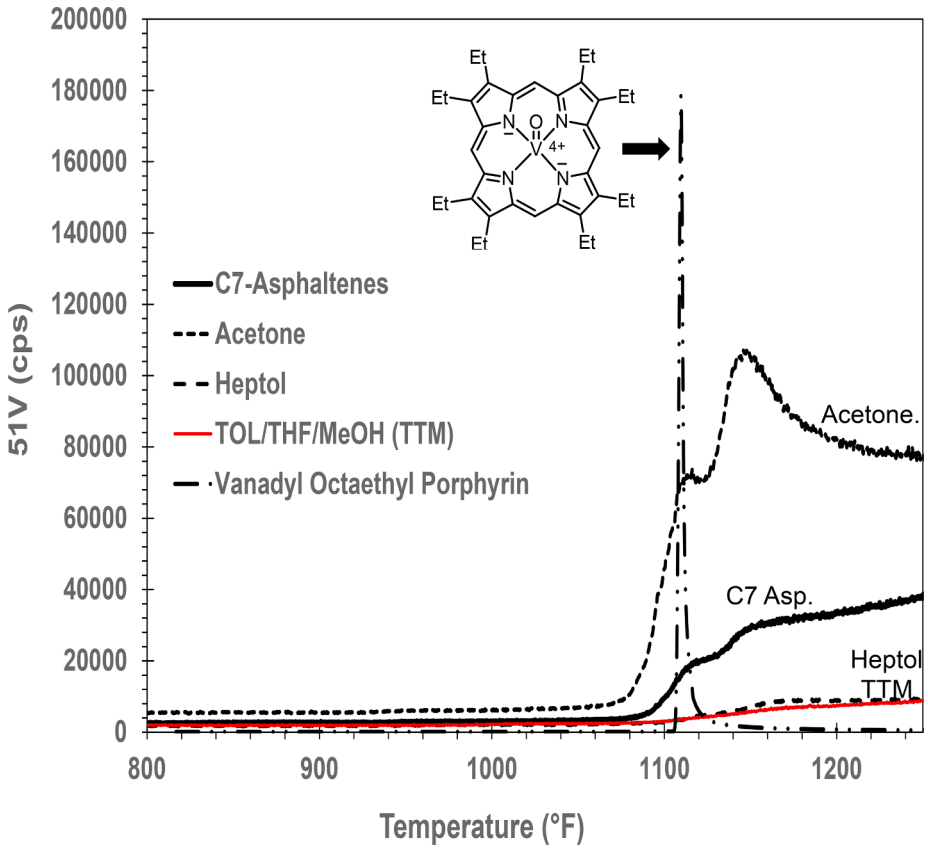

Fig. 6. GC trace of the vanadium signal (^{51}V in count per seconds) versus boiling temperature (°F) for the n-heptane (C7), acetone, heptol, and Toluene/THF/Methanol (TTM) extracted asphaltenes for Venezuelan crude oil 1. The results for the Venezuelan Crude 2 and NIST SRM 8505 are reported in Fig. 5S and Fig. 6S of the Supplementary Material.

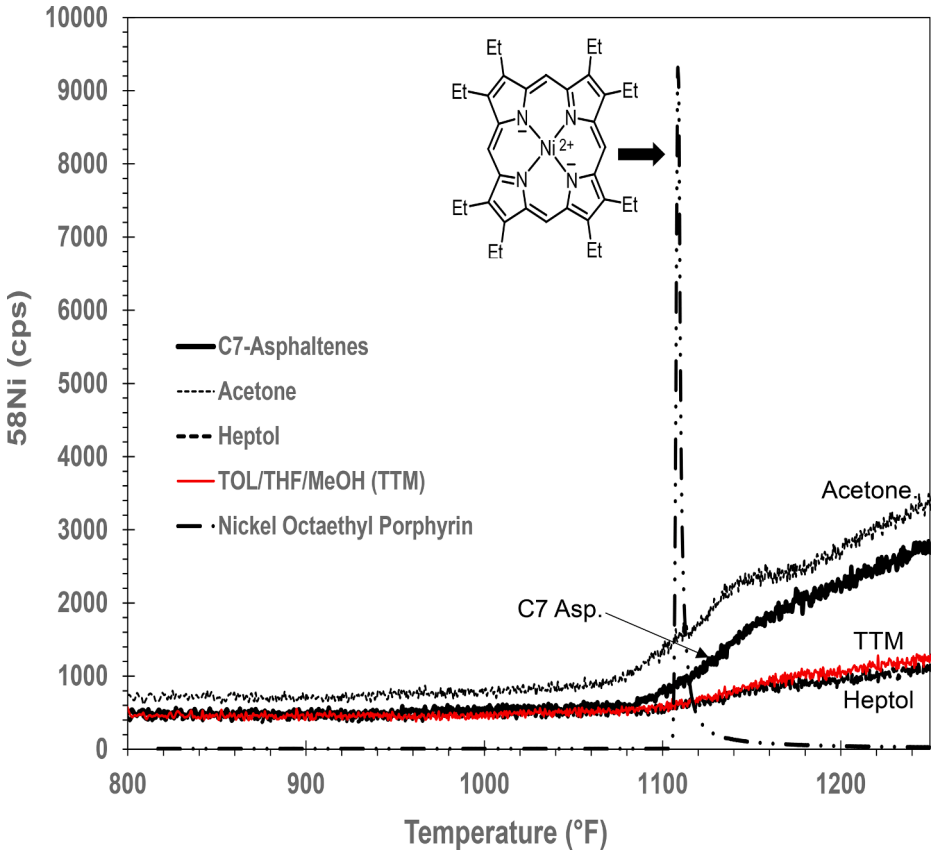

Fig. 7. GC trace of the nickel signal (^{58}Ni in count per seconds) versus boiling temperature (°F) for the n-heptane (C7), acetone, heptol, and Toluene/THF/Methanol extracted asphaltenes for Venezuelan crude oil 1. The results for the Venezuelan Crude 2 and NIST SRM 8505 are reported in Fig. 7S and Fig. 8S of the Supplementary Material.

contents increased in going from acetone to heptol and TTM asphaltenes. However, the asphaltene fractions from Venezuelan Crude **2** did not follow the same pattern, perhaps due to the irreversible absorbed species on the silica.

3.2. Asphaltene characterization

The characterization of the asphaltene fractions was carried out by solubility profile and size exclusion chromatography. Fig. 4 shows the asphaltene solubility profile for the n-heptane (C7 whole asphaltenes), acetone, heptol, and Toluene/THF/Methanol (TTM) extracted asphaltenes from the Venezuelan crude oil 1. As seen, the C7 "whole/unfractionated" asphaltenes have three "bumps" that seem to correspond with the three solvent-extracted fractions. The first signal at ~ 13.4 min is attributed to the acetone asphaltenes, at ~ 14.5 min to the heptol asphaltenes, and at 15.4–15.6 min to the TTM asphaltenes. Thus, the curves of the three solvent-extracted fractions are displaced toward the right, which suggests that their solubility decreased in the following order:

$$\text{Acetone Asphaltenes} > \text{Heptol Asphaltenes} > \text{TTM Asphaltenes} \quad (1)$$

Thus, the order showed in eq. 1 indicates how soluble the fraction is in hydrocarbons [61,62], i.e., the more displaced to the right, the less soluble the fraction. These results agree with the data discussed in the previous section and reported in Table 1. In general, the H/C ratio increase, and the nitrogen and sulfur contents decrease from acetone to TTM as described eq. 1. Similar tendencies have been reported previously for solubility fractions obtained for diverse samples using a different set of solvents [63,64]. The results for the Venezuelan crude **2** and NIST SRM 8505 are reported in Fig. 1S, and Fig. 2S of the Supplementary Material, and similar patterns were observed.

Asphaltene solutions in dichloromethane (1000 mg kg^{-1}) were analyzed by size exclusion chromatography (SEC) using a Mixed E column and 90/10 dichloromethane /methanol. Fig. 5 shows the SEC of the n-heptane (C7), acetone, heptol, and Toluene/THF/Methanol extracted asphaltenes for Venezuelan crude oil 1. The latter two fractions showed shorter elution times (presumably stronger aggregation) than acetone (evidence of free molecules / possible interaction with the column) [65,66]. Similar results were obtained for the Venezuelan crude 2 and NIST SRM 8505 (see Fig. 3S and Fig. 4S of the Supplementary Material). As in the previous publication, [33] elemental analysis, solubility profile, and SEC results suggest that fraction elution in SEC is strongly correlated to higher hydrogen deficiency and increased heteroatom levels. Similar findings were found in the Ni and V boiling point distributions, as shown in the next section.

3.3. Metal distribution function of boiling point by HTGC-ICPMS

As mentioned, understanding vanadium and nickel distributions in asphaltenes is crucial to address and mitigate the issues caused by these refractory petroleum fractions from upstream to downstream and synthesize specialty products. In this section, High-Temperature Gas Chromatography coupled with Inductively Coupled Plasma Mass Spectrometry (HTGC-ICP-MS) was used to determine metal distributions as a function of boiling points. To accomplish this task, the intensities of ^{51}V and ^{58}Ni vs. retention times were monitored, and the correlations of the retention time axis to the boiling points were achieved using a C-8 to C-100n-alkanes standard. Vanadium and nickel distributions for the asphaltene fractions of Venezuelan crude oil 1 are featured in Figs. 6 and 7, respectively

Table 3
Vanadium concentration and recovery for Venezuelan crude 1, calculated by GC-ICP-MS.

Sample	Vanadium Concentration (mg/Kg^{-1})[a]	Recovery (wt.%)[b]
C7-Asphaltene	866	47
Acetone	1098	62
Heptol	427	23
TTM	360	20

[a] Measured by GC-ICP-MS
[b] Percentage of recovery by weight using the elemental analysis reported inTable 1

The ^{51}V trace of the C7- and acetone asphaltenes reveal (Fig. 6) a broad bimodal shape, having the first peak around ~ 1100–1120 °F, and the second one with higher intensity, around ~ 1140–1160 °F. Similar behavior was observed for the Entrained C5 Maltenes and the In-Between C5-C7 asphaltenes in our previous publication.[33] The significant broadening of the signals suggests a remarkable higher complexity for molecules present in these fractions.

As shown in Fig. 6, the reference compound 2,3,7,8,12,13,17,18-octaethyl-21H, 23H-porphyrin vanadium oxide (OE-Etio-VO) showed the vanadium signal (~1110 °F) relatively close to the first peaks found in the C7 and acetone asphaltene fractions. This finding might suggest the presence of potentially dealkylated counterparts of the OE-Etio-VO type compound.[33,50] However, these asphaltene fractions are too complex to make a definitive assertion. Conversely, the heptol and Toluene/THF/Methanol extracted asphaltenes from Venezuelan crude oil 1 showed very small and broad vanadium signals starting ~ 1200 °F, suggesting that only a small fraction is distillable below 1300 °F (Fig. 6). Similar behaviors were observed for the Venezuelan crude 2 and SRM NIST 8505 as depicted in Fig. 5S and 6S.

Fig. 7 shows the GC trace of the ^{58}Ni signal versus boiling temperature (°F) for the n-heptane (C7), acetone, heptol, and Toluene/THF/Methanol extracted asphaltenes for Venezuelan crude oil 1. Analogous to the vanadium case, different ^{58}Ni signals are eluted depending on the extracting solvent. For the C7- and acetone asphaltenes, a broad peak is observed around 1140-1150F. This feature was not observed for the heptol and TTM asphaltenes.

Quantification of the metal contents below 1300 °F was attempted, focusing on vanadium. A calibration curve was made using the reference compound 2,3,7,8,12,13,17,18- octaethyl-21H, 23H-porphyrin vanadium oxide (OE-Etio-VO), setting the area integration from 1050 °F up to 1250 °F. Table 3 presents the calculated vanadium and recovery results for Venezuelan Crude 1, samples displayed in Fig. 6.

The results presented in Table 3 indicate that some vanadium is still in a distillable fraction, and its concentration is a function of the solvent used. As shown, we found that acetone is prone to concentrate more volatile vanadium-containing compounds than the other extrography fractions. It is well known that the majority of the metals are present in the non-distillable fraction (>1300°F) with less quantity in the distillable fraction, depending on the crude oil source. [67] Interestingly, the value determined by the acetone fraction for Venezuelan crude 1 (1097 mg kg^{-1}) is in the range measured for Boscan crude >1200°F cut, using conventional ICP-Optical Emission Spectroscopy (OES) analysis (1190 mg kg^{-1}). [67] We believe that the GC-ICP-MS data can be used as a first approximation of how much vanadium is present in the distillable range.

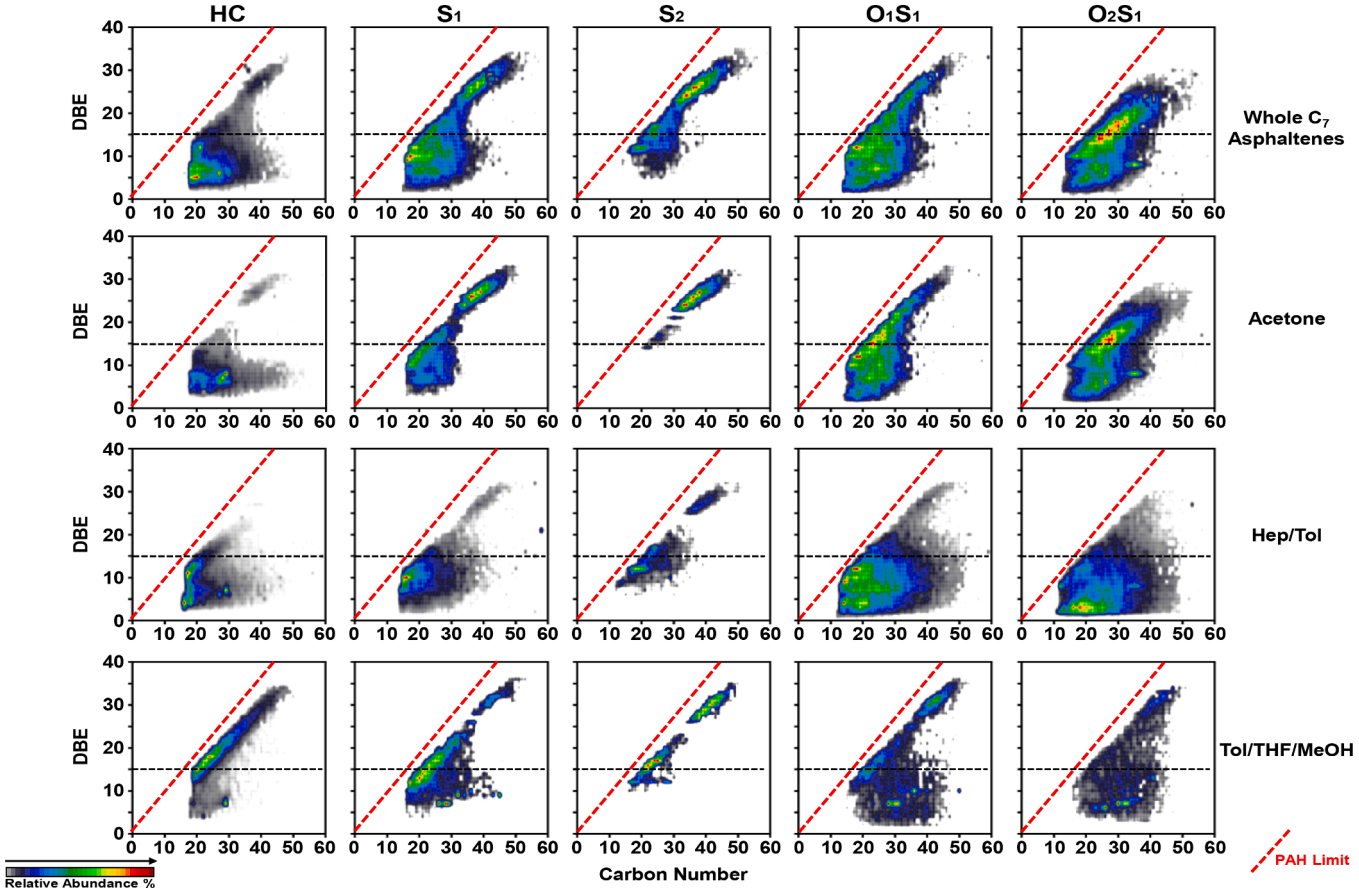

Fig. 8. DBE versus carbon number plots for whole C_7 asphaltenes obtained from Venezuelan crude 1 and the acetone, Hep/Tol, and Tol/THF/MeOH fractions for HC, S_1, S_2, O_1S_1, O_2S_1 classes. The color scale represents the relative abundance. The red dotted line highlights the polycyclic aromatic hydrocarbon limit, and a black dotted line has been included to facilitate sample comparison based on DBE. (For interpretation of the references to color in this figure legend, the reader is referred to the web version of this article.)

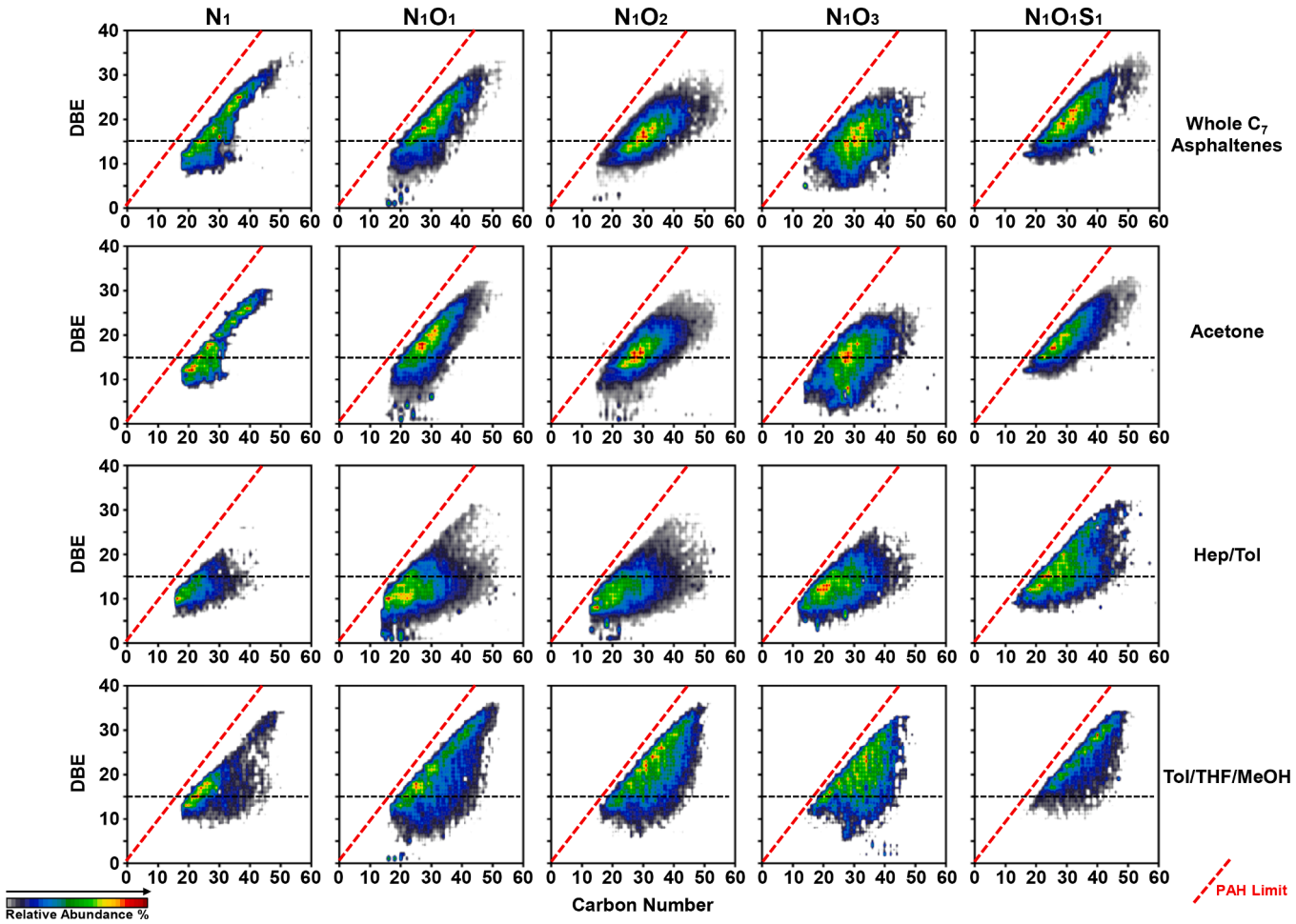

Fig. 9. DBE versus carbon number plots for whole C_7 asphaltenes obtained from Venezuelan crude 1 and the acetone, Hep/Tol, and Tol/THF/MeOH fractions, for N_1, N_1O_1, N_1O_2, N_1O_3, and $N_1O_1S_1$ classes. The color scale represents the relative abundance, the red dotted line highlights the polycyclic aromatic hydrocarbon limit, and a black dotted line has been included to facilitate sample comparison based on aromaticity. (For interpretation of the references to color in this figure legend, the reader is referred to the web version of this article.)

3.4. FT-ICR MS characterization

Ultra-high resolution mass spectrometry serves as a molecular-level elemental analyzer. It provides the exact mass for tens of thousands of detected ions and thus, enables the assignment of a unique molecular formula to each detected peak. However, ultra-high mass accuracy and resolving power is not the only requirement to access the "complete" molecular composition of ultra-complex mixtures such as heavy petroleum. Chemical separations, e.g., extrography, chromatography, and differential precipitation, are required to mitigate the effects of selective ionization [68]. In other words, APPI FT-ICR MS is not inherently quantitative because the myriad of species present within the samples reveals vastly different ionization efficiencies. Thus, analysis of whole/unfractionated samples only reveals limited information. Separations help mitigate the effects of selective ionization and have allowed for the detection of compounds that remained inaccessible during the study of the entire samples. For instance, in the case of naphthenic acids, solid-phase extraction on aminopropyl silica gel, using an eluotropic gradient with sequentially increased hydrophobicity, made possible the detection of naphthenic acids with higher carbon number and higher aromaticity. [69]

In the case of asphaltenes, extrography separation has facilitated the identification of archipelago/multicore compounds and asphaltene molecules with atypical low aromaticity but high heteroatom content. In the extrography method, asphaltenes are adsorbed on silica gel using a low mass loading ($\leq$10 mg of sample per gram of SiO_2) and then extracted, via Soxhlet extraction, with 1) acetone, 2) Hep/Tol 1/1, and 3) Tol/THF/MeOH. Fig. 8 presents the molecular composition, as accessed by (+) APPI FT-ICR MS, of whole Venezuelan crude oil 1 asphaltenes and its acetone, Hep/Tol, and Tol/THF/MeOH fractions.

In Fig. 8, the composition is represented as plots of double bond equivalent (DBE = number of rings plus double bonds to carbon) versus carbon number for selected compound classes. For instance, the class S_1 groups all the detected ions (radical cations and protonated molecules) comprised of carbon, hydrogen, and one sulfur atom. The class O_2S_1 contains species with C, H, two O atoms, and one S atom. A higher DBE suggests a higher "aromaticity" (more rings and double bonds). Furthermore, at constant DBE, an increase in carbon number indicates a higher content of CH_2 units (more alkyl substitution). Fig. 8 reveals several features:

- For whole asphaltenes and the first two extrography fractions, hydrocarbons with no heteroatoms (HC class) have predominant low DBE values (<15) and low carbon number (<30), which suggest the presence of remnant coprecipitated/occluded hydrocarbons within the samples.
- The prevalence of low DBE / low carbon number compounds is also evident for the S_1 class; however, whole asphaltenes and the acetone fraction reveal a greater abundance of highly aromatic compounds with DBE values above 20.

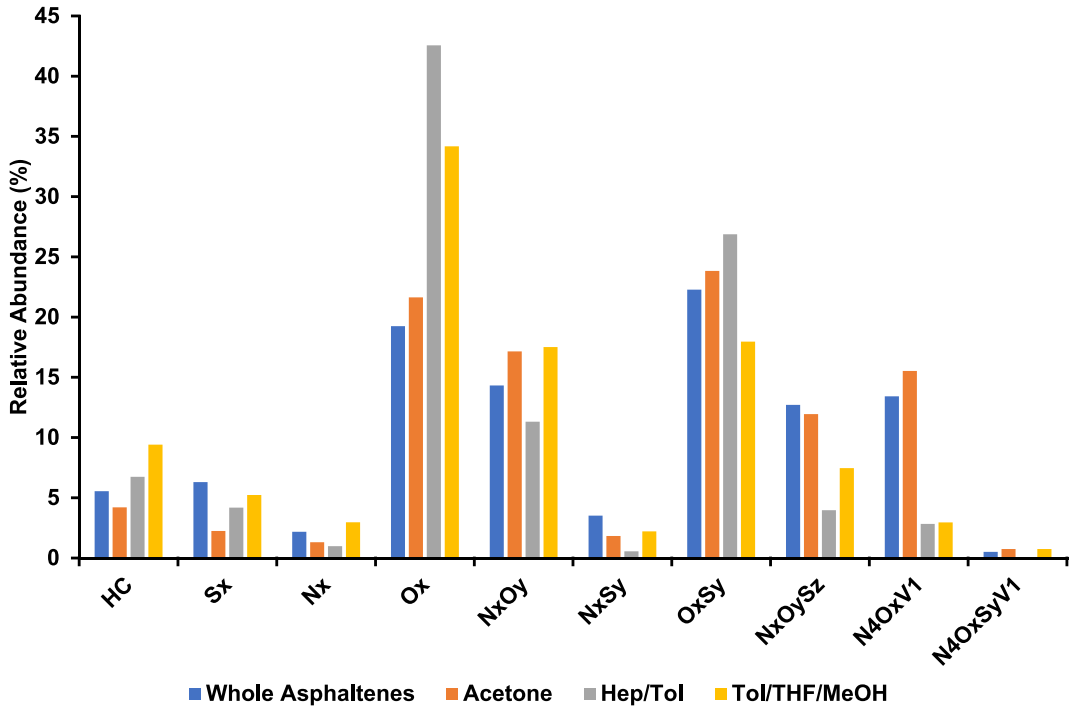

Fig. 10. Heteroatom class distribution for whole asphaltenes isolated from Venezuelan crude oil 1 and their extrography fractions.

- Compound classes with higher heteroatom content, such as S_2, O_1S_1, and O_2S_1, reveal highly aromatic species close to the polycyclic aromatic hydrocarbon (PAH) limit, which is known as a compositional boundary for fossil fuels. [70] The PAH limit suggests that aromatic/alkyl-depleted petroleum molecules with a "quasi" planar molecular structure should have DBE values not exceeding the ~ 90% of their carbon number. Molecules beyond this limit adopt geometries like fullerenes. In the DBE vs. carbon number plots, species close to the PAH line are very aromatic (peri condensed) and contain limited CH_2 units. Thus, the results indicate that S_2 compounds are very aromatic and feature little alkyl substitution for whole asphaltenes and the three extrography fractions.
- For whole asphaltenes and the acetone fraction, oxygenated S-containing compounds reveal increased abundances of highly aromatic species close to the PAH limit. However, they also present low DBE compounds, which are more prevalent for the Hep/Tol fraction. Previous studies suggest that low-DBE/heteroatom rich asphaltenes are alkane insoluble/toluene soluble ("asphaltene definition") likely because they contain heteroatomic functionalities capable of strong intermolecular interactions; thus, they exhibit strong aggregation regardless of their low aromaticity.
- The Tol/THF/MeOH fraction reveals HC and S_1 species with much higher aromaticity and limited alkyl chain content (clustered along with the PAH limit).
- The acetone fraction resembles the composition of the whole sample. Previous reports have demonstrated that acetone produces abundant non-aggregated ions in APPI. [36] Thus, its efficient ionization as "monomers" facilitates their detection in APPI FT-ICR MS analysis. Conversely, Hep/Tol and Tol/THF/MeOH reveal a much lower ionization efficiency. It has been suggested that the stronger aggregation of Hep/Tol and Tol/THF/MeOH is one of the causes for their decreased production of non-aggregated ions in APPI. Fig. 9S and 10S in the Supporting Information include the DBE vs. Carbon number plots for the samples derived from the Venezuelan crude 2 and the NIST SRM 8505 standard petroleum. The results suggest similar trends to the ones described above. It should be noted that oxygenated S-containing species for asphaltenes from Venezuelan crude 2 (Tol/THF/MeOH fraction) reveal distinct bimodal compositional ranges, with overall low DBE values (between 2 and 7), which suggest a mixture of functionalities: high DBE species (DBE $\geq$ 9) likely contain thiophene/furan moieties, whereas low DBE molecules should present "polar" functionalities such as sulfide, sulfoxide, thiols, carboxylic acid, and hydroxyls (widely reported/suggested for interfacial material isolated from asphaltenes). [71–73]

Fig. 9 presents the DBE vs. carbon number plots for N-containing compounds, with and without oxygen. The data indicate that N-containing molecules tend to be more aromatic. Again, the results reveal that acetone species resemble the composition of the whole sample. Furthermore, Hep/Tol and Tol/THF/MeOH present compositions with slightly lower aromaticity and abundant species closer to the PAH limit. Fig. 11S and 12S present the data corresponding to asphaltenes derived from the Venezuelan oil 2 and the NIST standard.

In general, data for "crude oil 2″ (Fig. 11S) indicates that whole asphaltenes and the acetone fraction feature similar compositional ranges, with abundant compounds close to the PAH limit, which suggests high aromaticity. Furthermore, Hep/Tol and Tol/THF/MeOH present longer homologous series (compounds with the same DBE but varying content of carbon atoms), which indicates a much higher content of more alkyl-substituted aromatic cores. On the other hand, samples derived from NIST standard asphaltenes seem to be depleted in N-containing compounds (Figure 12S).

Fig. 10 presents the heteroatom group distribution for the Venezuelan crude oil 1, in which the molecular formulas were grouped according to their heteroatom content. For instance, the group *Sx* comprises S_1, S_2, S_3, S_4, and S_5 compound classes. In general, the extrography fractions from Venezuelan crude oil 1 asphaltenes appear to get enriched in Ox species as a function of solubility/aggregation trend (as revealed by solubility profiles and GPC, Figs. 4 and 5).

The acetone fraction (Fig. 10) shows abundant vanadyl porphyrins (with and without sulfur) compared with Hep/Tol and Tol/THF/MeOH; however, based on the quantitative data presented in Table 1, all three extrography fractions have a similar concentration of vanadium (1930,

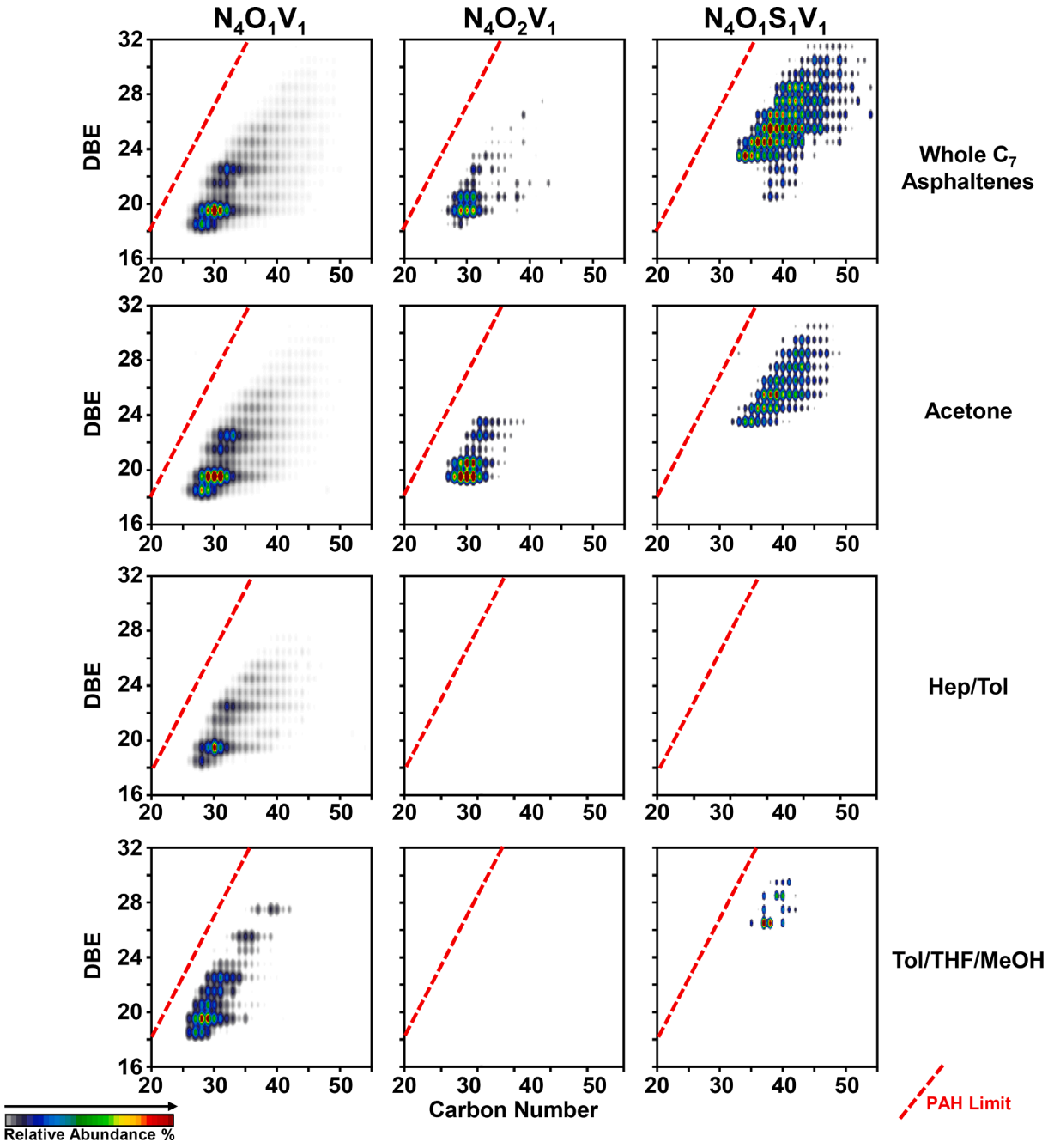

Fig. 11. DBE versus carbon number plots for vanadyl porphyrins ($N_4O_1V_1$) with and without additional O/S atoms ($N_4O_2V_1$, $N_4O_1S_1V_1$), for whole asphaltenes isolated from Venezuelan crude oil 1 and the respective extrography fractions.

1880, and 1760 ppm for Acetone, Hep/Tol, and Tol/THF/MeOH, respectively). Thus, the vanadium concentration within the samples does not account for the ~ 5.5-fold increase in the relative abundance of vanadyl porphyrins ($N_4O_xV_1$ class) for the acetone fraction. Previous studies have suggested that aggregation and intrinsic molecular features (e.g., aromaticity) affect the production efficiency of ions in APPI. Furthermore, the boiling point limit for vaporization before ionization in APPI is unknown and hypothesized around 1300F.

The data presented in previous sections suggest that the acetone fraction is prone to concentrate more volatile vanadium-containing compounds, revealing a higher solubility/weaker aggregation (Fig. 4), as was confirmed by GC-ICP-MS, data presented in Table 3. These differences in relative abundances for V-containing compounds are likely due, in part, to the extremely low volatility of the Hep/Tol and Tol/THF/MeOH fractions.

Figure 13S and 14S in the Supporting Information present similar trends, for the heteroatom group distribution (i.e., vanadyl porphyrins), for Venezuelan crude oil 2, and the NIST SRM 8505 standard. Additionally, GC-ICP-MS data shown in Table 3, also explain why it is so difficult to observe V and Ni in the other fractions. The decreased ionization efficiency could be due to a combination of the high boiling point of these molecules combined with strong aggregation and high ionization potentials intrinsic to molecular electronic structure.

Fig. 11 presents the compositional range for vanadyl porphyrins. Whole asphaltenes and acetone reveal the highest number of species (582 and 459 formulas, respectively), compared with Hep/Tol and Tol/THF/MeOH fractions (236 and 140 formulas). Vanadyl porphyrins with an additional oxygen atom

($N_4O_2V_1$) remain in the compositional range of the class $N_4O_1V_1$, which suggests that the extra oxygen atom is likely incorporated in a pendant group that causes no increase in DBE/carbon number (e.g., hydroxyl). However, there is an average increase of six DBE units when sulfur is present, suggesting direct sulfur incorporation as a benzothiophene pendant group. Figure 15S and 16S in the supporting information present the data for Venezuelan crude oil 2 and the NIST standard and demonstrate similar compositional trends when O/S-atoms are present.

Abundant nickel porphyrins were not identified in whole asphaltenes and the extrography fractions, regardless of the confirmed presence of this metal by bulk elemental analysis and the qualitative characterization by HTGC-ICP-MS. We hypothesize that increased concentration/ionization efficiency for vanadium and irreversible adsorption of Ni on SiO_2 could originate this result. In this regard, Combariza *et al.* [74] reported the effect of the used ionization source on detecting nickel and vanadyl porphyrins in heavy petroleum. The authors concluded that APPI usually enables complex mass spectra where peaks from high-ionization-energy (IE) compounds, with abundant heteroatoms ($N_xO_yS_z$), prevail and suppress metalloporphyrins Ni-containing species. Conversely, ionization via matrix-assisted laser desorption ionization (MALDI), with novel matrixes for electron transfer reactions, produces a less complex spectrum, with 4-fold fewer radical cations compared to APPI, in which nickel and vanadyl porphyrins are dominant. Thus, MALDI FT-ICR MS reveals fewer ions per nominal mass, dramatically improving signal resolution, mass accuracy, and dynamic range for difficult-to-detect species, such as nickel porphyrins. Thus, future efforts will focus on accessing molecular-level differences for Ni and V = O porphyrins via targeted ionization.

One of the most interesting results is the acetone fractions' boiling point distribution compared to whole asphaltenes. For crude oil 1 (Table 3), C7 asphaltenes reveal 47% of the vanadium in the distillable region (<1300F), whereas acetone presents 62%. This finding suggests that the extrography separation disrupts cooperative interactions and yields an extrography fraction, acetone, with weaker intermolecular interactions, which translates into weaker aggregation (as revealed by GPC), increased solubility, and lower boiling points. Once "acetone molecules" are extracted, the remaining compounds (present in heptol and TTM fractions) experience much stronger intermolecular interactions, which decreases their solubility and boiling point and increases their aggregation tendency. Thus, it is likely that difficulties in ionization by APPI for these problematic extrography fractions arise from aggregation and increased boiling point, as APPI features a boiling point limit hypothesized around 1300F.

4. Conclusion

- C7-Asphaltenes were separated by extrography on SiO_2 using acetone, heptol (n-heptane/toluene 1:1 vol), and a mixture of toluene, THF, and methanol (TTM). As in our previous work, [33] it was found that solubility and aggregation are strongly correlated to a higher hydrogen deficiency and increased heteroatom levels.
- The qualitative analysis of the spent silica by LIBS confirmed that different elements are present on the surface. Ni and V porphyrin molecules present on such feeds were preferentially adsorbed to the Si, presumably associated with the acidic sites.
- The GC-ICP-MS analysis of C7 Asp and the fractions shows that the vanadium and nickel compounds have boiling points starting at 1050 °F. A bimodal behavior was found for vanadium compounds present at the acetone fraction and the parent C7 ASP, where the first peak centered around 1110 °F very close to the 2,3,7,8,12,13,17,18-octaethyl-21H, 23H-porphyrin vanadium oxide (OE-Etio-VO), ~1110 °F, and the second centered around 1150 °F. This bimodal behavior is likely correlated to the bi/multimodal distribution of aromaticity for the N4O1V1 class as detected by APPI FT-ICR MS. Quantification of the vanadium content below 1300 °F for the Venezuelan crude 1, was carried out using the reference compound 2,3,7,8,12,13,17,18- octaethyl-21H, 23H-porphyrin vanadium oxide (OE-Etio-VO). The results showed that the acetone fraction contains a large amount of distillable vanadium present (~62 %) compared to only 47% for whole C7 asphaltenes.
- The acetone fraction showed more vanadyl porphyrins (with and without sulfur) than Hep/Tol and Tol/THF/MeOH. It is prone to concentrate more volatile vanadium-containing compounds, revealing a higher solubility/weaker aggregation, as is confirmed by GC-ICP-MS quantitative analysis. Similar trends for the heteroatom group distribution (i.e., vanadyl porphyrins) are observed for Venezuelan crude oil 2, and the NIST SRM 8505 standard. These results suggest that the extrography method is useful to produce a fraction enriched with asphaltene species that feature lower boiling points, higher solubility, weaker aggregation, and based on several reports, increased amounts of island structural motifs, which could be of interest for future carbon-based materials applications.

CRediT authorship contribution statement

Martha L. Chacón-Patiño: Conceptualization, Writing – original draft. **Jenny Nelson:** Resources, Investigation. **Estrella Rogel:** Methodology, Formal analysis. **Kyle Hench:** Resources, Investigation. **Laura Poirier:** Resources, Investigation. **Francisco Lopez-Linares:** Methodology, Formal analysis. **Cesar Ovalles:** Conceptualization, Supervision, Writing – original draft, Formal analysis.

Declaration of Competing Interest

The authors declare that they have no known competing financial interests or personal relationships that could have appeared to influence the work reported in this paper.

Acknowledgements

We thank Chevron Technical Center for providing funding and permission to publish this paper. Our appreciation to the Products & Technology Unit and the Global Laboratory management for their support.

A portion of this work was performed at the National High Magnetic Field Laboratory, supported by the National Science Foundation Cooperative Agreement No. DMR-1644779 and the State of Florida

Appendix A. Supplementary data

Supplementary data to this article can be found online at https://doi.org/10.1016/j.fuel.2021.122939.

References

[1]] Huc A, Argillier J-F, Renard G, Quignard A, Alazard N. Heavy Crude Oils; From geology to upgrading, an overview. 2011.
[2] Ramirez-Corredores MM. The Science and Technology of Unconventional Oils: Finding Refining Opportunities. In: The Science and Technology of Unconventional Oils. Elsevier; 2017. p. 1–40. https://doi.org/10.1016/B978-0-12-801225-3.00001-2.
[3] C. Ovalles Subsurface Upgrading of Heavy Crude Oils and Bitumen 1 CRC Press Boca Raton : CRC Press, Taylor & Francis Group, 2019.
[4] Gray MR. Upgrading Oilsands Bitumen and Heavy Oil. 1st ed. Edmonton, Alberta: The University of Alberta Press; 2015.
[5] J.G. Speight The Chemistry and Technology of Petroleum 0 CRC Press.
[6] Gawrys KL, Blankenship GA, Kilpatrick PK. On the Distribution of Chemical Properties and Aggregation of Solubility Fractions in Asphaltenes. Energy Fuels 2006;20(2):705–14.
[7] Rytting BM, Harper MR, Edmond KV, Zhang Y, Kilpatrick PK. High-Purity Vanadyl Petroporphyrins: Their Aggregation and Effect on the Aggregation of Asphaltenes. Energy Fuels 2020;34(1):164–78.
[8] Putman JC, Moulian R, Smith DF, Weisbrod CR, Chacón-Patiño ML, Corilo YE, et al. Probing Aggregation Tendencies in Asphaltenes by Gel Permeation Chromatography. Part 2: Online Detection by Fourier Transform Ion Cyclotron Resonance Mass Spectrometry and Inductively Coupled Plasma Mass Spectrometry.

Energy Fuels 2020;34(9):10915–25. https://doi.org/10.1021/acs.energyfuels.0c02158.
[9] Alboudwarej H, Svrcek W, Yarranton H, Akbarzadeh K. Asphaltene Characterization: Sensitivity of Asphaltene Properties to Extration Techniques. Can. Int. Pet. Conf., Petroleum Society of Canada 2001. https://doi.org/10.2118/2001-063.
[10] del Carmen GM, Chiaravallo N. Asphaltenes Deposition Control in Lake Maracaibo Crude Oil Production. SPE Int. Symp. Oilf. Chem., Society of Petroleum Engineers 2001. https://doi.org/10.2118/65009-MS.
[11] Ancheyta J, Trejo F, Rana MM. Asphaltenes. Chemcial Transformation during Hydroprocessing of Heavy Oils. Boca Raton. CRC Press; 2009.
[12] Ovalles C, Rogel E, Lopez J, Pradhan A, Moir M. Predicting reactivity of feedstocks to resid hydroprocessing using asphaltene characteristics. Energy Fuels 2013;27(11):6552–9. https://doi.org/10.1021/ef401471v.
[13] Ali MF, Abbas S. A Review of Methods for the Demetallization of Residual Fuel Oils. Fuel Proc Tech 2006;87(7):573–84.
[14] Rogel E, Ovalles C, Pradhan A, Leung P, Chen N. Sediment formation in residue hydroconversion processes and its correlation to asphaltene behavior. Energy Fuels 2013;27(11):6587–93. https://doi.org/10.1021/ef401614a.
[15] Sundaram KM, Mukherjee U, Baldassari M. Thermodynamic Model of Sediment Deposition in the LC-FINING Process †. Energy Fuels 2008;22(5):3226–36. https://doi.org/10.1021/ef800264e.
[16] Wandas R. Structural Characterization of Asphaltenes from Raw and Desulfurized Vacuum Residue and Correlation Between Asphaltene Content and the Tendency of Sediment Formation in H-oil Heavy Products. Pet Sci Technol 2007;25(1-2):153–68. https://doi.org/10.1080/10916460601054305.
[17] Ovalles C, Rogel E, Morazan H, Moir ME, Dickakian G. Method for Determining the Effectiveness of Asphaltene Antifoulants at High Temperature: Application to Residue Hydroprocessing and Comparison to the Thermal Fouling Test. Energy Fuels 2015;29(8):4956–65. https://doi.org/10.1021/acs.energyfuels.5b01360.
[18] Furimsky E. Chapter 7 Catalyst deactivation. In: Delmon, B. Yates JT, editor. Stud. Surf. Sci. Catal., 2007, p. 141–216. https://doi.org/10.1016/S0167-2991(07)80228-X.
[19] J. Ancheyta J.G. Speight Hydroprocessing of Heavy Oils and Residua 1st ed. 2007 CRC Press 10.1201/9781420007435.
[20] Barbier J, Marques J, Caumette G, Merdrignac I, Bouyssiere B, Lobinski R, et al. Monitoring the Behaviour and Fate of Nickel and Vanadium Complexes during Vacuum Residue Hydrotreatment and Fraction Separation. Fuel Process Technol 2014;119:185–9.
[21] Zuo P, Qu S, Shen W. Asphaltenes: Separations, structural analysis and applications. J Energy Chem 2019;34:186–207. https://doi.org/10.1016/j.jechem.2018.10.004.
[22] Wang L, Zhou Y, Qiu J. Influence of pore structures on the electrochemical performance of asphaltene-based ordered mesoporous carbons. Microporous Mesoporous Mater 2013;174:67–73. https://doi.org/10.1016/j.micromeso.2013.02.024.
[23] Park JG, Yun NG, Park YB, Liang R, Lumata L, Brooks JS, et al. Single-walled carbon nanotube buckypaper and mesophase pitch carbon/carbon composites. Carbon N Y 2010;48(15):4276–82. https://doi.org/10.1016/j.carbon.2010.07.037.
[24] Xiao N, Zhou Y, Ling Z, Qiu J. Synthesis of a carbon nanofiber/carbon foam composite from coal liquefaction residue for the separation of oil and water. Carbon N Y 2013;59:530–6. https://doi.org/10.1016/j.carbon.2013.03.051.
[25] Lee KS, Park M, Choi S, Kim J-D. Preparation and characterization of N, S-codoped activated carbon-derived asphaltene used as electrode material for an electric double layer capacitor. Colloids Surfaces A Physicochem Eng Asp 2017;529:107–12. https://doi.org/10.1016/j.colsurfa.2017.05.052.
[26] George Bohnert DEB. Methods of Making Carbon Fiber from Asphaltenes. Patent App. No 20140175688A1, 2014.
[27] Qu W-H, Guo Y-B, Shen W-Z, Li W-C. Using Asphaltene Supermolecules Derived from Coal for the Preparation of Efficient Carbon Electrodes for Supercapacitors. J Phys Chem C 2016;120(28):15105–13. https://doi.org/10.1021/acs.jpcc.6b0513610.1021/acs.jpcc.6b05136.s001.
[28] Baran D, Yardim MF, Atakül H, Ekinci E. Synthesis of carbon foam with high compressive strength from an asphaltene pitch. New Carbon Mater 2013;28(2):127–32. https://doi.org/10.1016/S1872-5805(13)60071-2.
[29] McLean JD, Kilpatrick PK. Comparison of Precipitation and Extrography in the Fractionation of Crude Oil Residua. Energy Fuels 1997;11(3):570–85.
[30] Acevedo N, Moulian R, Chacón-Patiño ML, Mejia A, Radji S, Daridon J-L, et al. Understanding Asphaltene Fraction Behavior through Combined Quartz Crystal Resonator Sensor, FT-ICR MS, GPC ICP HR-MS, and AFM Characterization. Part I: Extrography Fractionations. Energy Fuels 2020;34(11):13903–15. https://doi.org/10.1021/acs.energyfuels.0c02687.
[31] Chacón-Patiño ML, Rowland SM, Rodgers RP. Advances in Asphaltene Petroleomics. Part 2: Selective Separation Method That Reveals Fractions Enriched in Island and Archipelago Structural Motifs by Mass Spectrometry. Energy Fuels 2018;32(1):314–28.
[32] Chacón-Patiño ML, Rowland SM, Rodgers RP. Advances in Asphaltene Petroleomics. Part 3. Dominance of Island or Archipelago Structural Motif Is Sample Dependent. Energy Fuels 2018;32(9):9106–20. https://doi.org/10.1021/acs.energyfuels.8b01765.
[33] Chacón-Patiño ML, Nelson J, Rogel E, Hench K, Poirier L, Lopez-Linares F, et al. vanadium and nickel distributions in Pentane, In-between C5–C7 Asphaltenes, and heptane asphaltenes of heavy crude oils. Fuel 2021;292:120259. https://doi.org/10.1016/j.fuel.2021.120259.
[34] Chacón-Patiño ML, Rowland SM, Rodgers RP. Advances in Asphaltene Petroleomics. Part 1: Asphaltenes Are Composed of Abundant Island and Archipelago Structural Motifs. Energy Fuels 2017;31(12):13509–18.
[35] Chacón-Patiño LM, Rowland MS, Rodgers PR. The Compositional and Structural Continuum of Petroleum from Light Distillates to Asphaltenes: The Boduszynski Continuum Theory As Revealedby FT-ICR Mass Spectrometry. American Chemical Society 2018. https://doi.org/10.1021/bk-2018-1282.ch006.
[36] Chacón-Patiño ML, Moulian R, Barrère-Mangote C, Putman JC, Weisbrod CR, Blakney GT, et al. Compositional Trends for Total Vanadium Content and Vanadyl Porphyrins in Gel Permeation Chromatography Fractions Reveal Correlations between Asphaltene Aggregation and Ion Production Efficiency in Atmospheric Pressure Photoionization. Energy Fuels 2020;34(12):16158–72. https://doi.org/10.1021/acs.energyfuels.0c0334910.1021/acs.energyfuels.0c03349.s001.
[37] Ballard DA, Chacón-Patiño ML, Qiao P, Roberts KJ, Rae R, Dowding PJ, et al. Molecular Characterization of Strongly and Weakly Interfacially Active Asphaltenes by High-Resolution Mass Spectrometry. Energy Fuels 2020;34(11):13966–76. https://doi.org/10.1021/acs.energyfuels.0c02752.
[38] Boduszynski M. Petroleum Molecular Composition Continuity Model. Anal Methods Pet Upstream Appl 2015:3–30. https://doi.org/10.1201/b18109-3.
[39] McKenna AM, Chacón-Patiño ML, Weisbrod CR, Blakney GT, Rodgers RP. Molecular-Level Characterization of Asphaltenes Isolated from Distillation Cuts. Energy Fuels 2019;33(3):2018–29. https://doi.org/10.1021/acs.energyfuels.8b0421910.1021/acs.energyfuels.8b04219.s001.
[40] Pinkston DS, Duan P, Gallardo VA, Habicht SC, Tan X, Qian K, et al. Analysis of Asphaltenes and Asphaltene Model Compounds by Laser-Induced Acoustic Desorption/Fourier Transform Ion Cyclotron Resonance Mass Spectrometry. Energy Fuels 2009;23(11):5564–70. https://doi.org/10.1021/ef9006005.
[41] Yakubov MR, Milordov DV, Yakubova SG, Borisov DN, Gryaznov PI, Mironov NA, et al. Features of the composition of vanadyl porphyrins in the crude extract of asphaltenes of heavy oil with high vanadium content. Pet Sci Technol 2016;34(2):177–83. https://doi.org/10.1080/10916466.2015.1122627.
[42] Chacón-Patiño ML, Vesga-Martínez SJ, Blanco-Tirado C, Orrego-Ruiz JA, Gómez-Escudero A, Combariza MY. Exploring Occluded Compounds and Their Interactions with Asphaltene Networks Using High-Resolution Mass Spectrometry. Energy Fuels 2016;30(6):4550–61. https://doi.org/10.1021/acs.energyfuels.6b0027810.1021/acs.energyfuels.6b00278.s001.
[43] Fan S, Liu He, Wang J, Chen H, Bai R, Guo A, et al. Microwave-assisted Petroporphyrin Release from Asphaltene Aggregates in Polar Solvents. Energy Fuels 2020;34(3):2683–92. https://doi.org/10.1021/acs.energyfuels.9b03494.
[44] Oropeza D, González J, Chirinos J, Zorba V, Rogel E, Ovalles C, et al. Elemental Analysis of Asphaltenes Using Simultaneous Laser-Induced Breakdown Spectroscopy (LIBS)–Laser Ablation Inductively Coupled Plasma Optical Emission Spectrometry (LA-ICP-OES). Appl Spectrosc 2019;73(5):540–9.
[45] Casey J, Gao Y, Robert Thomas WY. New Approaches in Sample Preparation and Precise Multielement Analysis of Crude Oils and Refined Petroleum Products Using Single-Reaction-Chamber Microwave Digestion and Triple-Quadrupole ICP-MS. Spectroscopy 2016;31:11–22.
[46] Chacón-Patiño ML, Niles SF, Marshall AG, Hendrickson CL, Rodgers RP. Role of Molecular Structure in the Production of Water-Soluble Species by Photo-oxidation of Petroleum. Environ Sci & Technol 2020;54(16):9968–79. https://doi.org/10.1021/acs.est.0c01158.
[47] Chacón-Patiño ML, Smith DF, Hendrickson CL, Marshall AG, Rodgers RP. Advances in Asphaltene Petroleomics. Part 4. Compositional Trends of Solubility Subfractions Reveal that Polyfunctional Oxygen-Containing Compounds Drive Asphaltene Chemistry. Energy Fuels 2020;34(3):3013–30. https://doi.org/10.1021/acs.energyfuels.9b04288.
[48] Rogel E, Ovalles C, Vien J, Moir M. Asphaltene Solubility Properties by the In-Line Filtration Method. Energy Fuels 2015;29(10):6363–9. https://doi.org/10.1021/acs.energyfuels.5b01682.
[49] Ellis J, Rechsteiner C, Moir M, Wilbur S. Determination of volatile nickel and vanadinum species in crude oil and crude oil fractions by gas chromatography coupled to inductively coupled plasma mass spectrometry. J Anal At Spectrom 2011;26:1674–8. https://doi.org/10.1039/C1JA10058K.
[50] M.M. Boduszynski C.E. Rechsteiner M.E. Moir D. Leong J. Nelson L. Poirier et al. From a Dream to a Fact: Direct Measurement of Vanadium and Nickel Distribution in Crude Oil Cuts Fraction vol. 1282 2018 (800–1250 °f) 10.1021/bk-2018-1282.ch005.
[51] Cesar Ovalles CERJ, editor. The Importance of Mass Balances. Case Studies: Evaluation of Asphaltene Dispersants and Antifoulants. Anal. Methods Pet. Upstream Appl., 2018.
[52] R.E. Russo, X.L. Mao, J. Yoo J. JG. Laser Ablation. In: J.P. Singh, editor. Laser Induc. Break. Spectrosc, Elsevier, Amsterdam; 2007, p. 49–82.
[53] J.P. Singh SNT. Laser-Induced Breakdown Spectroscopy. Elsevier; 2007. https://doi.org/10.1016/B978-0-444-51734-0.X5001-7.
[54] Anabitarte F, Cobo A, Lopez-Higuera JM. Laser-Induced Breakdown Spectroscopy: Fundamentals, Applications, and Challenges. ISRN Spectrosc 2012;2012:1–12. https://doi.org/10.5402/2012/285240.
[55] Sergio Musazzi (Editor) UP (Editor). Laser-Induced Breakdown Spectroscopy: Theory and Applications. 1st Ed. Springer Series in Optical Sciences, 182; 2014.
[56] J.P., Singh, SNT.. Laser-Induced Breakdown Spectroscopy. Elsevier 2020. https://doi.org/10.1016/C2018-0-03938-9.
[57] Bauer AJR, Buckley SG. Novel applications of Laser-Induced Breakdown Spectroscopy. Appl Spectrosc 2017;71(4):553–66.
[58] Chirinos JR, Oropeza DD, Gonzalez JJ, Hou H, Morey M, Zorba V, et al. Simultaneous 3-dimensional elemental imaging with LIBS and LA-ICP-MS. J Anal At Spectrom 2014;29(7):1292–8.

[59] Hou H, Cheng L, Richardson T, Chen G, Doeff M, Zheng R, et al. Three-dimensional elemental imaging of Li-ion solid-state electrolytes using fs-laser induced breakdown spectroscopy (LIBS). J Anal At Spectrom 2015;30(11):2295–302.
[60] Ovalles C, Rogel E, Moir M, Thomas L, Pradhan A. Characterization of heavy crude oils, their fractions, and hydrovisbroken products by the asphaltene solubility fraction method. Energy Fuels 2012;26(1):549–56. https://doi.org/10.1021/ef201499f.
[61] Rogel E, Ovalles C, Vien J, Moir M. Asphaltene content by the in-line filtration method. Fuel 2016;171:203–9. https://doi.org/10.1016/j.fuel.2015.12.064.
[62] Rogel E, Ovalles C, Moir M. Asphaltene stability in crude oils and petroleum materials by solubility profile analysis. Energy Fuels 2010;24(8):4369–74. https://doi.org/10.1021/ef100478y.
[63] Rogel E, Roye M, Vien J, Miao T. Characterization of Asphaltene Fractions: Distribution, Chemical Characteristics, and Solubility Behavior. Energy Fuels 2015;29(4):2143–52. https://doi.org/10.1021/ef5026455.
[64] Rogel E, Roye M, Vien J, Witt M. Equivalent Distillation: A Path to a Better Understanding of Asphaltene Characteristics and Behavior, 2018, p. 51–72. https://doi.org/10.1021/bk-2018-1282.ch003.
[65] Ortega LC, Rogel E, Vien J, Ovalles C, Guzman H, Lopez-Linares F, et al. Effect of Precipitating Conditions on Asphaltene Properties and Aggregation. Energy Fuels 2015;29(6):3664–74. https://doi.org/10.1021/acs.energyfuels.5b00597.
[66] Rogel E, Moir M. Effect of precipitation time and solvent power on asphaltene characteristics. Fuel 2017;208:271–80. https://doi.org/10.1016/j.fuel.2017.06.116.
[67] Altgelt KH, Boduszynski MM. Composition, and Analysis of Heavy Petroleum Fractions. New York: Marcel Dekker; 1994.
[68] Rodgers RP, Mapolelo M, Robbins WK, Chacón-Patiño ML, Putman JC, Niles SF, et al. Combating selective ionization in the high resolution mass spectral characterization of complex mixtures. Faraday Discuss 2019;218:29–51. https://doi.org/10.1039/C9FD00005D.
[69] Clingenpeel AC, Rowland SM, Corilo YE, Zito P, Rodgers RP. Fractionation of Interfacial Material Reveals a Continuum of Acidic Species That Contribute to Stable Emulsion Formation. Energy Fuels 2017;31(6):5933–9. https://doi.org/10.1021/acs.energyfuels.7b00490.
[70] Hsu CS, Lobodin VV, Rodgers RP, McKenna AM, Marshall AG. Compositional Boundaries for Fossil Hydrocarbons. Energy Fuels 2011;25(5):2174–8. https://doi.org/10.1021/ef2004392.
[71] Qiao P, Harbottle D, Tchoukov P, Wang Xi, Xu Z. Asphaltene Subfractions Responsible for Stabilizing Water-in-Crude Oil Emulsions. Part 3. Effect of Solvent Aromaticity. Energy Fuels 2017;31(9):9179–87. https://doi.org/10.1021/acs.energyfuels.7b01387.
[72] Yang F, Tchoukov P, Pensini E, Dabros T, Czarnecki J, Masliyah J, et al. Asphaltene Subfractions Responsible for Stabilizing Water-in-Crude Oil Emulsions. Part 1: Interfacial Behaviors. Energy Fuels 2014;28(11):6897–904. https://doi.org/10.1021/ef501826g.
[73] Yang F, Tchoukov P, Dettman H, Teklebrhan RB, Liu L, Dabros T, et al. Asphaltene Subfractions Responsible for Stabilizing Water-in-Crude Oil Emulsions. Part 2: Molecular Representations and Molecular Dynamics Simulations. Energy Fuels 2015;29(8):4783–94. https://doi.org/10.1021/acs.energyfuels.5b00657.
[74] Ramírez-Pradilla JS, Blanco-Tirado C, Hubert-Roux M, Giusti P, Afonso C, Combariza MY. Effect of the Ionization Source on the Targeted Analysis of Nickel and Vanadyl Porphyrins in Crude Oil. Energy Fuels 2021;35(18):14542–52. https://doi.org/10.1021/acs.energyfuels.1c01743.